American Journal of Civil Engineering and Architecture, 2023, Vol. 11, No. 4, 127-135
Available online at http://pubs.sciepub.com/ajcea/11/4/4
Published by Science and Education Publishing
DOI:10.12691/ajcea-11-4-4

Seismic Assessment of Historical Bridge: Numerical Modeling and Structural Evaluatione

Amin Bagherzadeh Azar[1,*], Ali Sari[2]

[1]Institute of Earthquake Engineering and Disaster Management, Istanbul Technical University, Istanbul, Turkey
[2]Faculty of Civil Engineering, Istanbul Technical University, Istanbul, Turkey
*Corresponding author: azar19@itu.edu.tr

Received October 20, 2023; Revised November 22, 2023; Accepted November 29, 2023

Abstract In this study a comprehensive survey using faro laser scanning is performed to create a realistic 3D geometry model for subsequent seismic analysis of the bridge. The seismic response of the bridge is investigated using macro modeling approach based on finite elements. The adaptation of the Concrete Damage Plasticity (CDP) material model for masonry units and the Mohr-Coulomb material model for the backfill have been implemented. Nonlinear dynamic analyzes were then performed to identify the most vulnerable areas of the bridge. The examination of the results in terms of contour plots of tensile damage and maximum displacements has provided a thorough description of the seismic response of the entire bridge. The methodology used in this study can be considered a comprehensive basis for evaluating the seismic response and failure of historic structures.

Keywords: *historical bridge, seismic analysis, FE model, bridge failure*

Cite This Article: Amin Bagherzadeh Azar, and Ali Sari, "Seismic Assessment of Historical Bridge: Numerical Modeling and Structural Evaluatione." American Journal of Civil Engineering and Architecture, vol. 11, no. 4 (2023): 127-135. doi: 10.12691/ajcea-11-4-4.

1. Introduction

Failure of infrastructure could result in significant direct and indirect costs to the economy and society and could hamper rescue and recovery efforts. Therefore, there is an urgent need to accurately assess the performance of ancient masonry infrastructures and to provide detailed and accurate data for the preservation and maintenance of these monuments. In recent years, several methods have been developed to predict the behavior of masonry arch bridges [1-5], but the difficulty of representing the behavior of the material requires the use of a simplified but effective structural model. It is necessary to verify the load-bearing capacity of masonry arch bridges with respect to seismic action in order to design the necessary strengthening measures. For example, failure studies after earthquakes have shown that out-of-plane reactions are one of the main reasons for the vulnerability of historic structures. unfortunately, a few studies have been conducted on the seismic evaluation of historical structures, that some approaches based on numerical tools [6-11] have been developed to explain the behavior of this type of structure. Fairfield [12] performed several tests on semicircular arches. The infill consisted of graded dry sand. Analysis of the results showed that the collapse load increased with the depth of the infill. Melbourne et al. [13] tested a full-scale model of a masonry arch bridge to identify the effect of spandrel walls and backfill material to the performance of the bridge. The failure occurred by a four-joint mechanism related to ring separation. It was additionally found that the backfill significantly decreased arch ring deformation. Royles et al. [14] studied the impact of backfill materials and spandrel walls on bridge ultimate strength. 24 arch bridges were studied for this purpose. The researchers discovered that reinforcing the spandrel walls increased the overall strength of the bridge. Stavroulaki et al [15] create a realistic geometric model to analyze a stone arch bridge using Ground Penetrating Radar (GPR). Macro and micro combination methods are used in the model. Haciefendioglu et al [16] have performed the analyzes of the historical bridge in the software TNO DIANA based on the finite element and macro modeling methods. Dall'Asta et al [17] developed a multidisciplinary approach to determine the seismic safety of historic structures. Laser scanning and associated point cloud processing were used to determine the exterior and interior shapes of the structure. Hokelekli et al [18] investigated the in-plane and nonlinear structural responses of the bridge spandrel walls of a historic bridge. ABAQUS structural software was used to create the finite element model of the bridge and perform the nonlinear seismic analysis. Kujawaa et al. [19] use ABAQUS software to study a historic church. The geometry is determined by laser scanning.

The objective of this research is to demonstrate the interface between laser scanning survey and structural analysis in order to obtain a more realistic output of structural behavior. Terrestrial laser scanning was used to precisely determine the geometry of the bridge. Using the point cloud data, a three-dimensional CAD-based solid

model of the structure was constructed. Following the bridge's numerical modeling, a nonlinear dynamic analysis was carried out. This method aids in identifying the most vulnerable components of ancient bridges that require strengthening to reduce seismic susceptibility.

2. Characteristic Features of the Case Study

The case study of the Halilviran Bridge is located in southern Turkey. Figure 1 and Figure 2 depict the plan sections and elevations, as well as the key geometric parameters of the bridge. The bridge was built during the Roman period [20,21] and has survived to the present day thanks to major interventions and restoration work throughout the Ottoman period. The bridge is made up of seven arches. The primary arch is a semicircular arch that rises from the rocky foundation. The structure's entire length is 132 meters, while the roadway's width is 5.10 meters. 8.50 meters is the vertical distance between the bridge and the ground. The arches' spans range from 5.95 m to 7.00 m from west to east. The seventh arch placed in the eastern direction, has a distinct shape from the previous arches. It has a pointed shape that is comparable to a round arch but is positioned at a lower height.

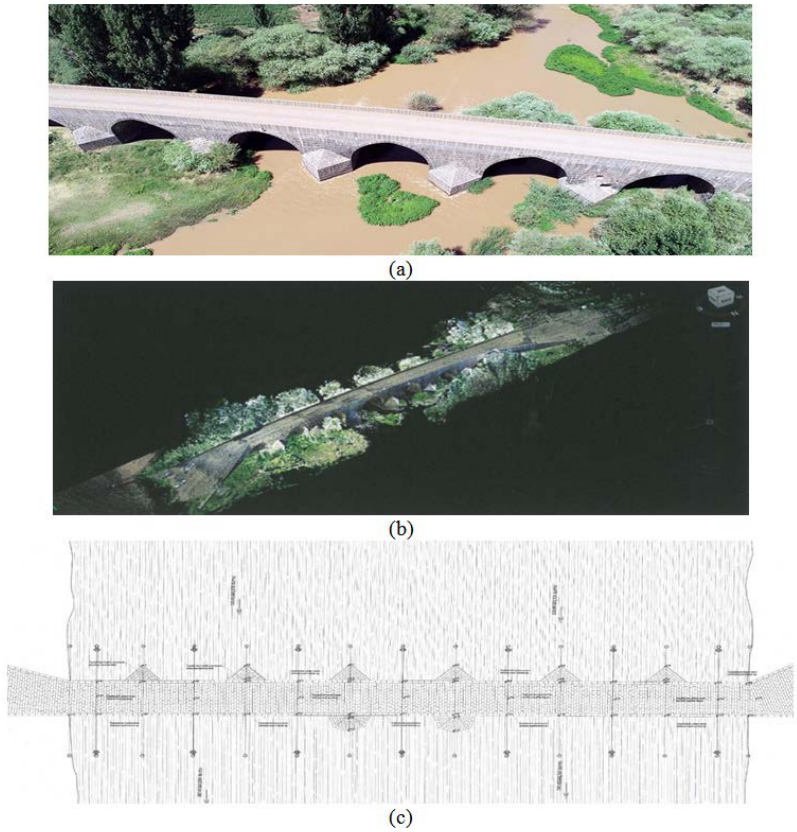

Figure 1. Halilviran Bridge: (a) Photo, (b) 3D Scanning cloud image and (c) CAD drawing [22].

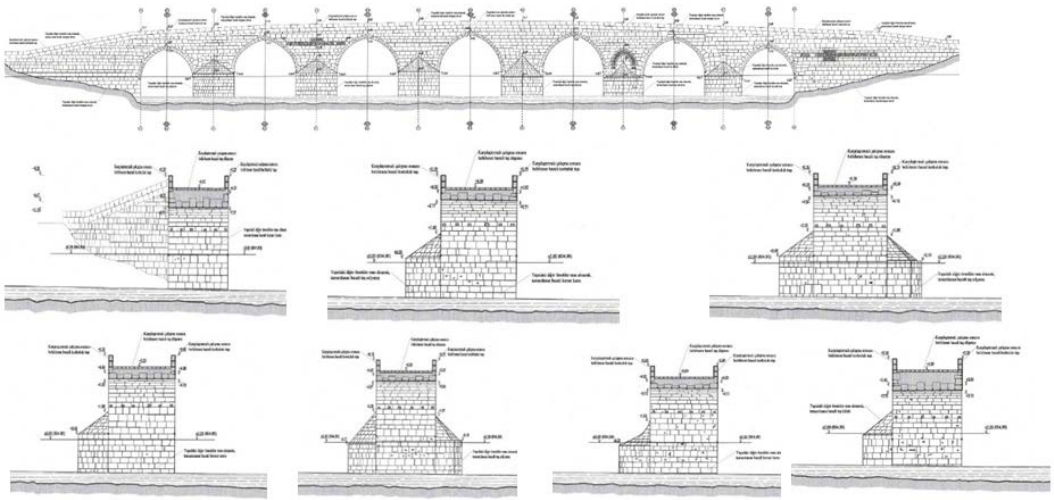

Figure 2. Halilviran Bridge. Section and elevation views with indication of the main geometrical dimensions [22].

Laser scanners have been used to digitize objects ranging in size from minimal diagnostic artifacts to massive, complicated monuments. Laser scanning technologies were employed in this investigation to inspect and document the bridge's as-built condition. It is a non-destructive, accurate method to collect the surface data on objects. These devices calculate the distance to an item using an infrared light beam and record it as data points with spatial coordinates. These data are then evaluated using various types of computer software to generate a detailed image with coordinates and dimensions. After scanning the bridge completely, the data is exported as a point cloud encompassing all visible aspects and actual bridge dimensions. This point cloud can then be transformed into the real shape of the object and exported to AutoCAD software, where two-dimensional (2D) (Figure 2) and three-dimensional (3D) (Figure 1.b) models of the bridge can be built.

3. FE Model and Adopted Material

The geometric characterization of the bridge based on available data, as well as accurate on-site inspections and extensive envision collections made by the authors, enabled the authors to define the bridge's 3D FE models. Figure 3 depicts a broad perspective of the bridge's geometric models, which were generated directly in Abaqus [23]. The model was made up of different macro-elements components (Figure 4). C3D8R, an 8-node reduced integration element, was used for the 3D FE model. In the context of nonlinear dynamic investigations, the element sizes were set with the aim of achieving both reliable results and computing efficiency. The structure's global reaction as well as the local responses of the individual macro elements were extensively analyzed. Furthermore, the interaction of bridge components is required for a realistic modeling of bridge reaction. Contact was assumed to have a thickness of zero, a coefficient of friction of 0.6 for tangential behavior, and a coefficient of friction of hard contact for normal surface-to-surface contact behavior, where hard contact refers to interaction without softening or penetration into the surface [24].

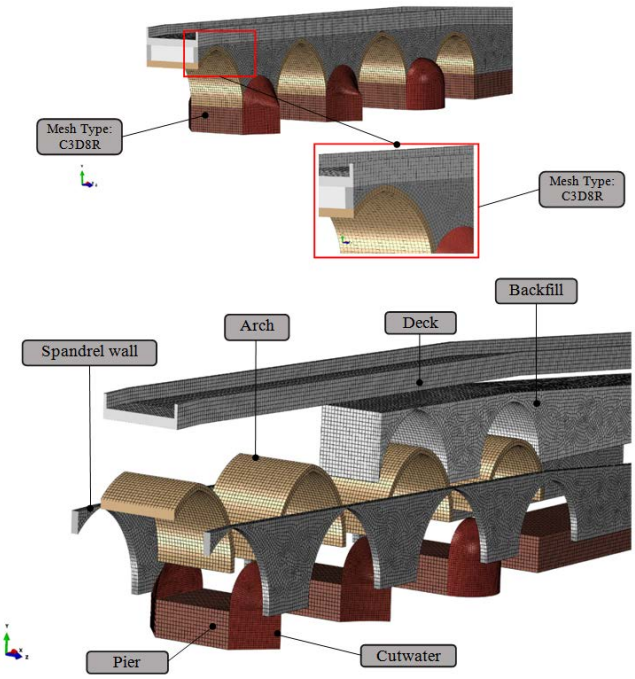

Figure 3. Finite element model of the half bridge

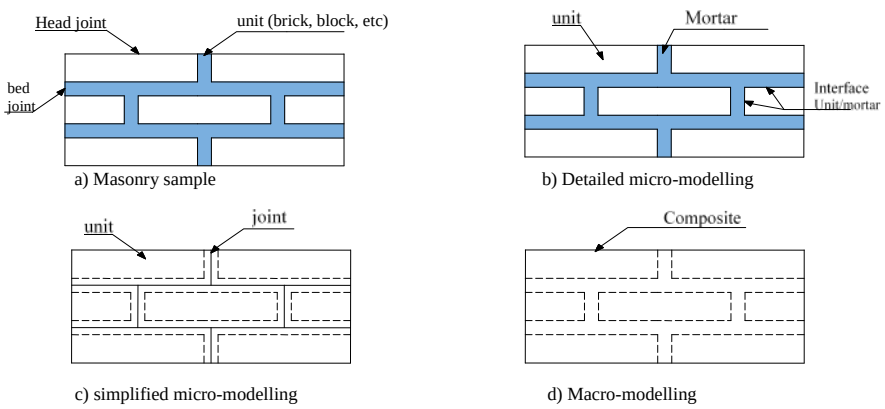

Figure 4. Material modeling techniques [25]

4. Concrete Damage Plasticity (CDP) Model

It is essential to precisely establish the material characteristics in order to precisely replicate the bridge's nonlinear behavior. The Concrete Damaged Plasticity (CDP) model was created to represent the inelastic behavior of masonry. This mechanical model is capable of simulating two failure modes, tensile cracking and compressive crushing, as well as material deterioration under cyclic loads. In terms of stress and strain, the CDP model can be stated as follows:

$$\sigma_t = (1-d_t) D_0^{el} : \left(\varepsilon - \varepsilon_t^{el}\right) \quad (1)$$

$$\sigma_c = (1-d_c) D_0^{el} : \left(\varepsilon - \varepsilon_c^{el}\right) \quad (2)$$

where σ_t is a tensile stress vector and σ_c is a compressive stress vector, plastic strains are represented ε_t^{el} and ε_c^{el} for tension and compression, respectively, d_t and d_c are variables representing damage in tension and compression, and D_0^{el} is the initial modulus of elasticity in the undamaged state. Lubliner et al. [26] provided the CDP yield function, which was updated by Lee & Fenves, [27] as follows:

$$F = \left(\sqrt{\frac{3}{2}}\sqrt{\bar{:}\, s}\right) - 3\alpha\, \bar{p} + \beta\, \hat{\bar{\sigma}}_{max} - \gamma\, \hat{\bar{\sigma}}_{max} - (1-\alpha)\bar{\sigma}_c = 0 \quad (3)$$

$$G_P = \sqrt{\left(\varepsilon \sigma_{t0} \tan\psi\right)^2 + \left(\frac{3}{2}\, s : s\right)} - \bar{p} \tan\psi \quad (4)$$

Where the deviatoric stress tensor and the maximal effective principal stress are represented by $\hat{\bar{\sigma}}_{max}, \bar{s}$. G_P is the potential (plastic) function that takes into account the dilation angle (ψ) in the plane of the mean stress-deviatoric stress, the uniaxial stress (σ_{t0}) at failure, and the eccentricity parameter (ε).

5. Mohr–Coulomb Constitutive Model

The fill material greatly influences the ultimate strength of masonry arch bridges. It often consists of soil, unbound masonry or crushed stone. The Mohr-Coulomb (M-C) constitutive model was employed in this investigation to incorporate the infill material model. Yielding occurs when the shear stress at any point in a material reaches a value that is linearly dependent on the normal stress in the same plane, according to the Mohr-Coulomb criteria. The M-C shear stress (τ) is a function of the normal stress (σ), cohesion (c), and friction (φ) plasticity models, which are represented as:

$$\tau = c + \sigma \tan \varnothing \quad (5)$$

The M-C model can be represented by three stress invariants. The equivalent pressure stress:

$$p = -\frac{1}{3} trace(\sigma) \quad (6)$$

The Mises equivalent stress:

$$q = \sqrt{\frac{3}{2}(S:S)} \quad (7)$$

And, deviatory stress:

$$r = (9(S*S:S))^{\frac{1}{3}} \quad (8)$$

Where $S = stressdeviator = \sigma + pl$.

In addition, M-C yield surface is:

$$F = R_{mc} q - p \tan\tan\varnothing - c = 0 \quad (9)$$

Where (R_{mc}) is deviatoric stress, q is Mises equivalent stress, p is equivalent pressure, $\varnothing(\theta, f^x)$ is friction angle which θ = temperature, $f^x, \alpha = 1,2,\ldots$ is predefined field variables and $c(\varepsilon^{-pl}\theta, f^x)$ is evolution of cohesion in the form of isotropic hardening that ε^{-pl} is equivalent plastic strain. The geognostic tests explored in the literature are used to determine mechanical characteristics, as shown in Table 1 through Table 4.

Table 1. Masonry material properties

Part	ρ (Kg/m^3)	E (Mpa)	υ
Pier	2500	2850	0.2
Cutwater	2100	1000	0.2
Arch	2100	3500	0.2
Spandrel wall	1900	1800	0.2
Deck	1900	1500	0.2

Note: E = Young's Modulus; ρ = Density; υ = Poisson's-Coefficient.

Table 2. CDP parameters

Specification	rate
(ψ)	15°
(ε)	0.1
f_{b0} / f_{c0}	1.16
K_c	0.667
Viscosity parameter	0.01

Table 3. M-C material parameters for the backfill

ρ (Kg/m^3)	E (N/mm^2)	υ	c (MPa)	$\varnothing$ (°)
1900	500	0.2	0.05	35

Table 4. Inelastic masonry parameters

Part	f_t (Mpa)	f_c (Mpa)	G_f (Mpa)
Pier	0.70	7	48
Arch	0.85	8.5	60
Side walls	0.30	3.5	22

Table 5. Dynamic characteristics of the bridges

Arches No.	Arches span (m)	The initial natural frequency (Hz)	
		Test Results	Results based on Eq.(10)
7	16	5.84	5.92
1	15.7	5.28	6.20
1	19.49	6.07	5.12
2	25.2	4.07	4.13
1	24.8	4.05	4.20
8	15	4.74	6.17
2	10	8.86	7.86
3	12	6.98	7.05

6. Eigenfrequency Analysis

To effectively predict structural behavior, finite element modeling is required. The initial finite element model in the context of masonry constructions must be validated using tests or empirical methods. Bayraktar et al. [27] employed statistical methods to establish a quantifiable association between the maximum arch span and the initial natural frequencies of masonry bridges based on an investigation of the natural frequencies, Eq.(10).

$$y = -3.935 ln ln(x) + 16.824 \quad (10)$$

where x and y are the maximum arch span and the first frequency, respectively. Table 5 shows the theoretical Eq. (10) and the experimentally determined values of the first frequency for eight historical bridges. The experimentally and theoretically values are close to each other, as indicated and the authors concluded that Eq. (10) can be used to validate the analytical model of masonry bridges. The maximum arch span of the Halilviran bridge is 7 m. The results of the theoretical Eq. (10) and the analytical model are 9.16 Hz and 8.80, respectively (Figure 5). It is confirmed that the finite element model accurately represents the real behavior of the structure, since the difference between the theoretical and the analytically determined values of the first frequency is insignificant.

Table 6. Time period and mass participation ratio in X-Y and Z direction

Mode	*T (s)*	*X (%)*	*Y (%)*	*Z (%)*
1	0.11	0	0	24.02
2	0.11	0	0	0.1
3	0.10	0.1	0	12.7
4	0.10	0.4	0	0
5	0.09	35.4	0	0
6	0.09	0.1	0	6.55
7	0.08	0	0	0.4
8	0.08	0	0	0.2
9	0.08	0	0	4.60
10	0.07	0	0	0.1

The distribution of the bridge's first 10 modes in longitudinal and transversal directions, as well as the corresponding periods and the participating mass ratio (PMR) along the principal directions, is shown in Table 6. The first and third mode forms, as stated, are effective in the modal behavior of the Halilviran bridge. The first mode (*f = 8.8076* Hz) affects the upper components of the bridge, the deck and the top of the parapet walls, with a PMR of 24.02% in the transverse direction. The third mode (*f = 12.70* Hz) involves the upper part of the piers and parapet walls with a PMR of 12.72% in the transverse direction, while the fifth mode (*f = 35.40* Hz) involves the infill and deck of the bridge with a PMR of 35.4% in the longitudinal direction.

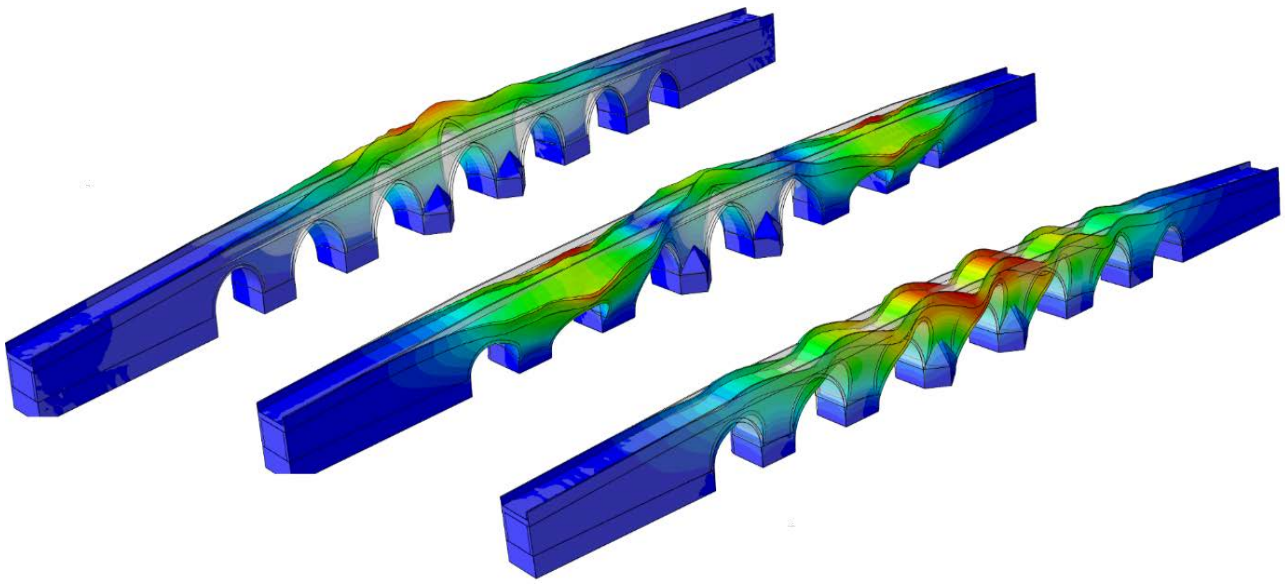

Mode 1, f_1 = 8.8076 Hz Mode 3, f_3 = 9.8325 Hz Mode 5, f_5 = 11.010 Hz

Figure 5. Halilviran Bridge. Distribution of the modes in the longitudinal and transversal directions. Deformed shapes of the first main modes, corresponding periods and participating mass ratios

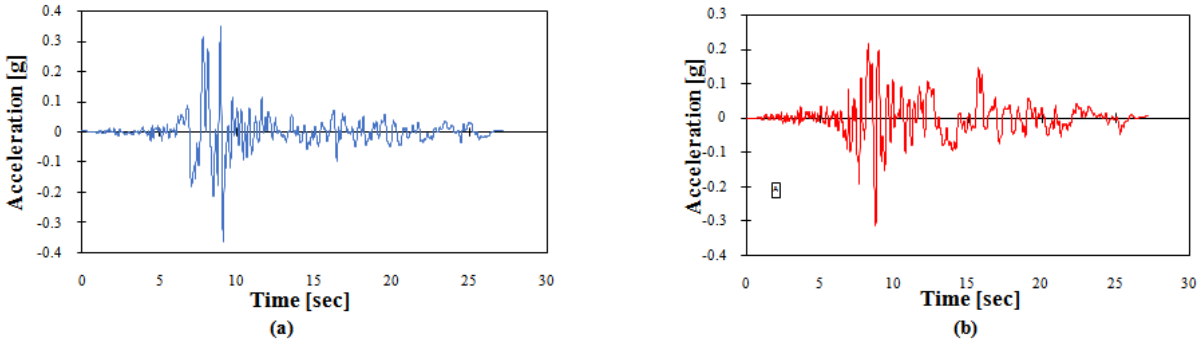

Figure 6. Horizontal components of the real accelerograms used in the non-linear dynamic analyses: (a) longitudinal direction and (b) transversal direction [29].

7. Nonlinear Dynamic Analyses

The nonlinear dynamic analyses are carried out in the software Abaqus Standard [23]. A static analysis is used to apply gravity loads first. Then, seismic behavior of the bridge is investigated using nonlinear dynamic analysis and actual acceleration data recorded during the Düzce earthquake sequence on August 17, 1999. Figure 6 depicts the acceleration time history, the two horizontal components, in relation to the 0.36g PGA in the longitudinal and transversal directions. The model is subjected to the Full Newton-Raphson method for solving nonlinear equilibrium equations using a step-by-step integration technique with a time increment of 0.005 s.

Due to the significant processing resources required for the analyses, it was assumed that the accelerograms would be limited to 5 seconds (between 7 and 12 seconds on the diagram).

8. Results

Damage in masonry is usually caused by tension stress, as it has relatively low tensile strength compared to compressive strength. Tensile failures form on bridges when the corresponding plastic strains and principal stresses under tension exceed the limit values. Figure 7 show the maximum values and distributions of equivalent plastic strains (PEEQT) in the bridge under combined significant longitudinal and transverse acceleration plotted at the end of the total duration of earthquake recordings, i.e., after 5 s. It was found that the plastic tensile strain in the model are concentrated in the areas near the interlocking of the wall and the arches.

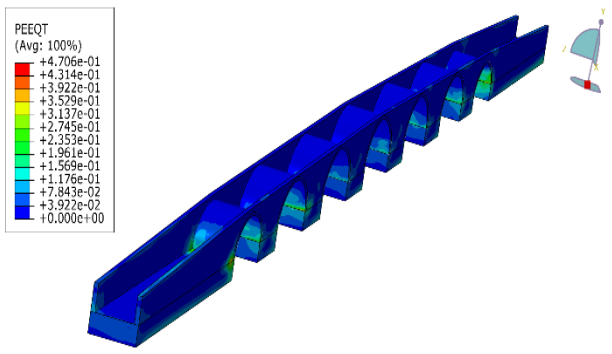

Figure 7. Maximum principal (tension) strain contour maps of the bridge.

Figure 10 shows the counter map of dynamic displacements in the transverse directions of the bridge spandrel walls, illustrating the importance of out-of-plane structural response in masonry bridges. Figure 8 and Figure 9 illustrate that the maximum principal stresses of the masonry along the spandrel walls interface, as well as the bridge arches while subjected to strong ground motion. Figure 11 and Figure 12 depicts the time-dependent variation in the minimum principal stresses and locations of concentrated stress.

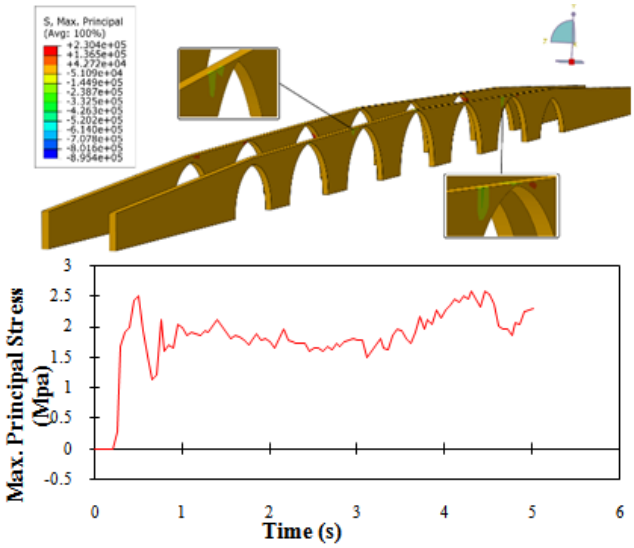

Figure 8. Maximum principal (tension) stress contour maps and time history of the spandrel walls

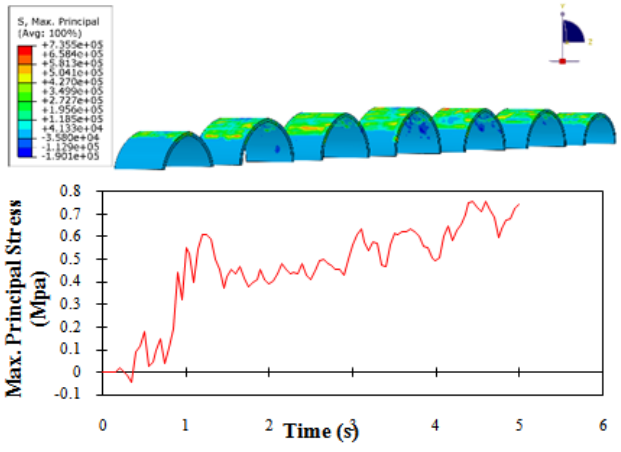

Figure 9. Maximum principal (tension) stress contour maps and time history of the arches

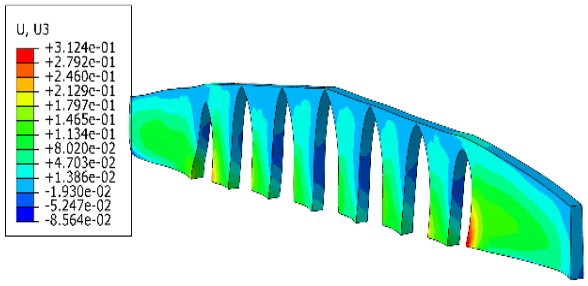

Figure 10. Total displacement contour maps of the transverse dynamic displacements for the spandrel wall

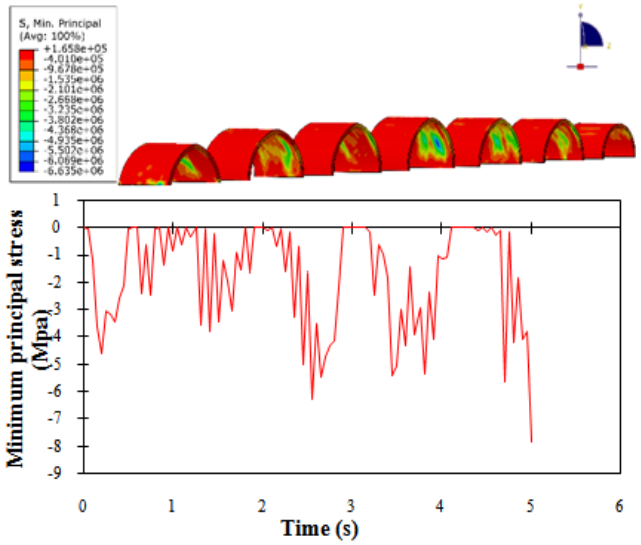

Figure 11. Minimum principal (compression) stress contour maps and time history of arches

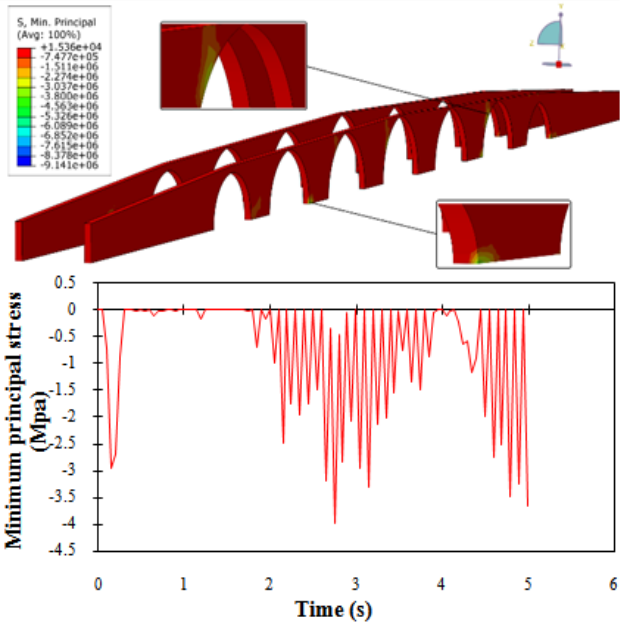

Figure 12. Minimum principal (compression) stress contour maps and time history of spandrel walls

9. Conclusion and Recommendations

- To study the seismic behavior of the bridge, the three-dimensional finite element (FE) model was developed. The FE effectively captures the complicated geometry of the bridge, which was determined by laser scanning. It was found that the point cloud obtained by terrestrial laser scanning provides fast and very accurate data for determining the structural geometry.
- The bridge exhibits a pronounced dynamic behavior, as shown by the preliminary analysis of its natural frequency. The bridge three primary modes characterized by high PMR, which affects the bridge overall structural integrity, due to the presence of masonry.
- The primary modes of the bridge have low periods, which leads to a significant amplification of the structural frequency and consequently to significant structural damage.
- The analysis of the plastic strain damage contour plots reveals that the bridge shows signs of damage, especially in the spandrel wall and the higher parts of the arches.
- The maximum principal stress and minimum principal stress of the arches do not reach the limited stress of 0.85 MPa and 8.5 MPa, respectively, but they are almost at the limit.
- The maximum principal stress and the minimum principal stress of the parapet walls reach the limited stress of 0.35 MPa and 3.5 MPa, respectively, in some parts of the walls.
- The spandrel walls exhibit out-of-plane responses in seismic behavior, which is one of the main reasons for masonry structures failure.
- In model, the 1st and 3rd mode shapes occurred in the transverse direction, whereas the and 5th mode shape occurred in the longitudinal direction.

Many masonry bridges have been designated as historical monuments, and they must be preserved using practical restoration techniques and appropriate materials for construction. It is critical to comprehend the construction's materials, structural components, and structural integrity. Some recommendations based on FE models are offered in the next section, and various restoration procedures based on field survey are discussed:

- In the case of transverse seismic activities, the collapse of the bridge may be heavily reliant on the out-of-plane mechanisms of the components, necessitating particular retrofitting procedures to assure the structure's monolithic behavior. As a result, it is critical to prioritize the repair and reinforcing of the old parapet walls that are vulnerable to these forces. Figure 10 shows the out-of-plane displacement of the spandrel wall of the Halilviran Bridge. To prevent out-of-plane failure of the spandrel walls, there are several ways to reinforce the stress areas. These techniques include using transverse bars to connect two spandrel walls, replacing the backfill with concrete fill, deconstructing and reconstructing the backfill with a tapered section, filling the backfill with grout, applying a thin concrete deck, and using a fabric-reinforced cement matrix (FRCM). All these techniques are suitable to improve the tensile behavior of the spandrel walls, resulting in strengthening of the bridge.

- filling material plays an important role in the reinforcement of bridges. Three effects are highlighted in the positive contribution of the infill material to the load-bearing capacity of a masonry arch bridge: The vertical dead load of the fill adds compressive stresses to the arch, which helps to its stability; it also enables for better distribution of traffic loads operating on the road surface to the arch's extrados, and, it effectively restrains the lateral movements of the arch by mobilizing the passive pressure. In this study, it was found that the backfill also has significantly wider compliant zones. Thus, by enhancing the mechanical qualities of the backfill, the bridge's seismic response was significantly improved. This is most noticeable in the rise in elastic modulus and cohesiveness.
- Water caused corrosion of the embedded rock and a loss of mechanical strength in the bridge's piers and abutments, according to an on-site investigation. Furthermore, vegetation was detected surrounding the bridge's piers (Figure 13). During an on-site assessment, this vegetation can conceal existing damage and is responsible for existing capillary cracking on the abutments and piers, both of which contribute to the degradation of the bridge and its components. Furthermore, several funguses (Figure 14) were detected on the stones. As water pierced the bridge's stonework, moisture deteriorated the piers and abutment stones even more. The field assessment also indicated that the mortar was of poor quality, allowing certain stones to be readily removed. Proper maintenance planning should be addressed to overcome these challenges. As a result, a reinforced concrete layer is being investigated for reinforcing and consolidating the bridge foundations. Repointing the mortar in the bridge's joints between the masonry pieces was considered. The mortar composition used to repoint the masonry joints must be carefully evaluated. The lime-based mortar should be as near to the color of the existing brickwork as feasible. These mortars should be as resistant to the region's harsh environmental circumstances (high humidity, contact with waves) as feasible while being compatible with original materials.
- The route of the bridge is paved with cut and fragile gravel stones. Vegetation had overrun the road. The current vegetation may aid in compaction, but it may also obstruct waterproofing and capillary drainage. The absence of adequate drainage will cause crystallization and subsequent rotting of steel anchors, which are one of the bridge's reinforcing measures, culminating in the disintegration of the load-bearing component. As a result, all masonry viaduct elements (arches, walls, and roadway) should be properly cleansed of efflorescence using high-pressure water. Almost all of the difficulties connected with a lack of waterproofing, such as parapet damage, moisture and water penetration, material deterioration, and mortar loss in joints, will be addressed by considering the drainage system.

Figure 13. Corrosion of the pier due to the presence of water

Figure 14. presence of fungus on the stone surfaces

Figure 15. presence of vegetation om roadway and spandrel walls

This study demonstrates how visual inspection, geometric laser scanning, and FE techniques can be used to assess the state of historical infrastructure. Visual inspection reveals major faults in various areas of the bridge; however, laser scanning offers accurate information about the outer layers and through FE model susceptible components that require reinforcement to withstand seismic loads are identified. It should be emphasized that appropriate care of historic bridges may ensure that these monuments continue functioning effectively for decades to come, thus it is vital to properly assess the status of a bridge in need of repair and choose the best course of action.

References

[1] P. J. Fanning, T. E. Boothby, and B. J. Roberts, "Longitudinal and transverse effects in masonry arch assessment," *Constr. Build. Mater.*, vol. 15, no. 1, pp. 51-60, 2001.

[2] A. Bayraktar and E. Hökelekli, "Seismic performances of different spandrel wall strengthening techniques in masonry arch bridges," *Int. J. Archit. Herit.*, vol. 15, no. 11, pp. 1722-1740, 2021.

[3] E. Erdogmus and T. E. Boothby, "Strength of spandrel walls in masonry arch bridges," *Transp. Res. Rec.*, vol. 1892, no. 1, pp. 47-55, 2004.

[4] S. Casolo, "Rigid element model for non-linear analysis of masonry façades subjected to out-of-plane loading," *Commun. Numer. Methods Eng.*, vol. 15, no. 7, pp. 457-468, 1999.

[5] D. M. Armstrong, A. Sibbald, C. A. Fairfield, and M. C. Forde, "Modal analysis for masonry arch bridge spandrell wall separation identification," *NDT \& E Int.*, vol. 28, no. 6, pp. 377-386, 1995.

[6] G. Lucibello, G. Brandonisio, E. Mele, and A. De Luca, "Seismic damage and performance of Palazzo Centi after L'Aquila earthquake: A paradigmatic case study of effectiveness of mechanical steel ties," *Eng. Fail. Anal.*, vol. 34, pp. 407-430, 2013.

[7] M. Valente and G. Milani, "Damage survey, simplified assessment, and advanced seismic analyses of two masonry churches after the 2012 Emilia earthquake," *Int. J. Archit. Herit.*, vol. 13, no. 6, pp. 901–924, 2019.

[8] M. Betti and A. Vignoli, "Numerical assessment of the static and seismic behaviour of the basilica of Santa Maria all'Impruneta (Italy)," *Constr. Build. Mater.*, vol. 25, no. 12, pp. 4308–4324, 2011.

[9] F. Clementi, A. Pierdicca, A. Formisano, F. Catinari, and S. Lenci, "Numerical model upgrading of a historical masonry building damaged during the 2016 Italian earthquakes: the case study of the Podestà palace in Montelupone (Italy)," *J. Civ. Struct. Heal. Monit.*, vol. 7, pp. 703–717, 2017.

[10] G. Castellazzi, A. M. D'Altri, S. de Miranda, and F. Ubertini, "An innovative numerical modeling strategy for the structural analysis of historical monumental buildings," *Eng. Struct.*, vol. 132, pp. 229–248, 2017.

[11] Jafari, Seyed Reza, and Majid Pasbani Khiavi. "Parametric Study of the Modal Behavior of Concrete Gravity Dam by Using Finite Element Method." Civil Engineering Journal 5.12 (2019): 2614-2625.

[12] C. A. Fairfield and D. A. Ponniah, "MODEL TESTS TO DETERMINE THE EFFECT OF FILL ON BURIED ARCHES.," *Proc. Inst. Civ. Eng. Build.*, vol. 104, no. 4, pp. 471–482, 1994.

[13] C. Melbourne and M. Gilbert, "The behaviour of multiring brickwork arch bridges," *Struct. Eng.*, vol. 73, no. 3, 1995.

[14] R. Royles and A. W. Hendry, "MODEL TESTS ON MASONRY ARCHES.(INCLUDES APPENDICES).," *Proc. Inst. Civ. Eng.*, vol. 91, no. 2, pp. 299–321, 1991.

[15] M. E. Stavroulaki, B. Riveiro, G. A. Drosopoulos, M. Solla, P. Koutsianitis, and G. E. Stavroulakis, "Modelling and strength evaluation of masonry bridges using terrestrial photogrammetry and finite elements," *Adv. Eng. Softw.*, vol. 101, pp. 136–148, 2016.

[16] K. Hac\iefendio\uglu, H. B. Ba\csa\uga, and S. Banerjee, "Probabilistic analysis of historic masonry bridges to random ground motion by Monte Carlo Simulation using Response Surface Method," *Constr. Build. Mater.*, vol. 134, pp. 199–209, 2017.

[17] A. Dall'Asta, G. Leoni, A. Meschini, E. Petrucci, and A. Zona, "Integrated approach for seismic vulnerability analysis of historic massive defensive structures," *J. Cult. Herit.*, vol. 35, pp. 86–98, 2019.

[18] E. Hokelekli and B. N. Yilmaz, "Effect of cohesive contact of backfill with arch and spandrel walls of a historical masonry arch bridge on seismic response," *Period. Polytech. Civ. Eng.*, vol. 63, no. 3, pp. 926–937, Sep. 2019, doi: 10.3311/PPci.14198.

[19] M. Kujawa, I. Lubowiecka, and C. Szymczak, "Finite element modelling of a historic church structure in the context of a masonry damage analysis," *Eng. Fail. Anal.*, vol. 107, p. 104233, 2020.

[20] C. Groot, P. J. M. Bartos, and J. J. Hughes, "Historic mortars: characteristics and tests-Concluding summary and state of the art," in *Proc. Of Int. RILEM workshop on Historic mortars: Characteristics and tests*, 2000, pp. 443-455.

[21] A. Moropoulou, A. Bakolas, P. Moundoulas, E. Aggelakopoulou, and S. Anagnostopoulou, "Strength development and lime reaction in mortars for repairing historic masonries," *Cem. Concr. Compos.*, vol. 27, no. 2, pp. 289-294, 2005.

[22] A. B. Azar and A. Sari, "Historical Arch Bridges-Deterioration and Restoration Techniques," *Civ. Eng. J.*, vol. 9, no. 7, 2023, doi: 10.28991/CEJ-2023-09-07-010.

[23] Dassault Systèmes Simulia, "Abaqus 6.12 analysis user's manual: Prescribed conditions, constraints & interactions," *Abaqus 6.12*, vol. 5, p. 831, 2012.

[24] M. Bolhassani, A. A. Hamid, A. C. W. Lau, and F. Moon, "Simplified micro modeling of partially grouted masonry assemblages," *Constr. Build. Mater.*, vol. 83, pp. 159–173, 2015.

[25] E. Hokelekli and B. N. Yilmaz, "Effect of cohesive contact of backfill with arch and spandrel walls of a historical masonry arch bridge on seismic response," *Period. Polytech. Civ. Eng.*, vol. 63, no. 3, pp. 926-937, 2019.

[26] J. Lubliner, J. Oliver, S. Oller, and Ejij. Onate, "A plastic-damage model for concrete," *Int. J. Solids Struct.*, vol. 25, no. 3, pp. 299–326, 1989.

[27] J. Lee and G. L. Fenves, "Plastic-damage model for cyclic loading of concrete structures," *J. Eng. Mech.*, vol. 124, no. 8, pp. 892–900, 1998.

[28] A. Bayraktar, T. Türker, and A. C. Altuni\csik, "Experimental frequencies and damping ratios for historical masonry arch bridges," *Constr. Build. Mater.*, vol. 75, pp. 234-241, 2015.

[29] "PEER Ground Motion Database - PEER Center." https://ngawest2.berkeley.edu/.